Automation in Construction 142 (2022) 104477

Contents lists available at ScienceDirect

Automation in Construction

journal homepage: www.elsevier.com/locate/autcon

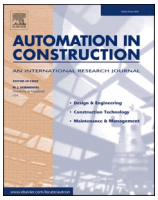

Robot-based mobile sensing system for high-resolution indoor temperature monitoring

Yang Geng [a,b,c], Mufeng Yuan [a,b,c], Hao Tang [a,b,c], Ye Wang [a,b,c], Ziliang Wei [a,b,c], Borong Lin [a,b,c,*], Weimin Zhuang [a,d]

[a] School of Architecture, Tsinghua University, Beijing 100084, China
[b] Key Laboratory of Eco Planning & Green Building, Ministry of Education, Tsinghua University, Beijing, China
[c] Beijing Key Laboratory of Indoor Air Quality Evaluation and Control, Tsinghua University, Beijing, China
[d] Architectural Design & Research Institute of Tsinghua University, Beijing, China

ARTICLE INFO

Keywords:
Indoor environmental quality (IEQ)
Air temperature
Mobile sensing
Robotics
Spatio-temporal distribution
Smart building

ABSTRACT

Indoor environmental quality (IEQ) monitoring is an important basis of smart buildings to ensure human comfort and control energy systems. IEQ monitoring conventionally relies on a limited number of stationary sensors deployed at selected locations, which has little capacity to capture fine spatial characteristics due to the cost of infrastructure and maintenance. This paper describes a robot-based mobile sensing system for high-resolution temperature monitoring by selecting air temperature as the targeted IEQ parameter. Experiments were conducted in a classroom to test the mobile sensing performance through comparisons with the dense stationary sensor network. Furthermore, two spatio-temporal processing methods were developed to reconstruct continuous thermal maps from short- and long-term monitoring. The results indicate that the robot velocity of 0.25–0.45 m/s is better than 0.60–0.80 m/s and 0.10–0.20 m/s, and that the proposed methods are suitable for generating accurate, high-resolution thermal maps.

1. Introduction

1.1. Background

The conventional building industry is challenged by strict demands of energy efficiency and the increasing complexity of the built environment [1]. Smart buildings with the capability to dynamically respond to climate, grids and users have been promoted in the past few decades [2,3]. Intelligent monitoring and analytics of various types of building performance data are fundamental prerequisites to achieve the goals of smart building [4]. Among all monitoring performances, indoor environmental quality (IEQ) is among the most important aspects because people spend about 90% time indoors, and IEQ directly influences human satisfaction, health and well-being [5–7]. Real-time IEQ monitoring helps to detect poor or unexpected conditions [8,9] and provides signals for the control of facilities, such as heating, ventilation and air-conditioning (HVAC) systems, to enhance IEQ performance and energy efficiency [10–12]. IEQ monitoring has thus become a major focus of many building rating systems such as BREEAM [13], LEED [14] and WELL [15] as well as measurement guidelines such as AHSRAE/CIBSE/USGBC Performance Measurement Protocols for commercial buildings [16].

Despite the importance of IEQ monitoring, its applications in real-life buildings are often inadequate for fully grasping IEQ information, which limits its value and effects on IEQ improvement and energy saving. The key challenge is the complex spatio-temporal distribution characteristics of IEQ due to the joint influences of outdoor climate, building envelopes, space layout, human activity, equipment and other indoor disturbances [17–20]. For example, Pollard et al. [17] found that the mean air temperature at different locations in a 1220 m^2 space varied by >3 °C at midday on workdays (spatial distribution), while Lee et al. [20] revealed that the temporal variation of CO_2 concentration could also have a wide range of approximately 400 ppm (parts per million; 1 ppm equals 1 ml/m^3) between 9 a.m. and 6 p.m. on the same day (temporal distribution).

The temporal issue in IEQ monitoring can be solved by current technology. Recent developments in the Internet of Things (IoT) and Wireless Sensor Networks (WSNs) [21,22] have enabled the emergence of a series of integrated, low-cost and intelligent IEQ monitoring systems

* Corresponding author at: School of Architecture, Tsinghua University, Beijing 100084, China.
E-mail address: linbr@tsinghua.edu.cn (B. Lin).

https://doi.org/10.1016/j.autcon.2022.104477
Received 4 March 2022; Received in revised form 30 June 2022; Accepted 3 July 2022
Available online 18 July 2022

[23,24]. These systems support simultaneous measurement of various IEQ parameters, wireless transmission, cloud storage and remote download, meaning that continuous, long-term IEQ data is now available at high-frequency intervals without much effort.

The spatial issue still lacks a cost-effective solution, however. To better understand spatial distribution characteristics, a common approach is to install multiple IEQ sensors at different positions. This method is generally defined as stationary sensing. Although stationary sensing makes sense in theory, it leads to three problems in practice. Firstly, more sensors mean more infrastructure investment costs. The affordability constraint often results in fewer sensors in applications than suggested to be used by guidelines and standards, which significantly reduces the spatial resolution of IEQ monitoring [25]. Secondly, due to the stationary sensor positions, each IEQ sensor can only represent a small space range around its installation location [26]. In other words, such stationary sensing method is highly sensitive to the selection of sensor locations [27]. The actual selection of sensor installation positions is often not as intended because of several practical issues, such as the requirement of connecting to an external power supply and non-invasion to the normal building operations. In large spaces in particular, IEQ sensors are usually placed on the perimeter of the floorplan [17], far away from where people actually congregate. Without a sufficient number of sensors and a representative sampling strategy, the IEQ data obtained by stationary sensing in these cases can only represent a limited area rather than the overall IEQ conditions throughout the building [22,23].

Thirdly, stationary sensing can only collect IEQ data 'passively' and lacks the agility necessary to 'actively' adapt to the changing environment. For example, personnel locations are likely to dynamically change in a building [28]. If we want to know the real-time IEQ conditions around people, then the stationary sensing method may fail when personnel locations are far from the preset static sensor locations.

Due to the above predicaments of stationary sensing, a new sensing paradigm is required to improve the spatial resolution and flexibility of IEQ monitoring: mobile sensing.

1.2. Literature review of mobile sensing

Mobile sensing can be used both outdoors and indoors. For outdoor contexts, researchers usually utilise humans (i.e. by using smartphones, smartwatches, wearable sensors and the like) or vehicles as mobile sensing platforms to collect various spatio-temporal data at the urban or neighbourhood scale. Chaix [29] discussed the potential of combining wearable sensors with the Global Positioning System (GPS), which can provide a mobile sensing perspective for understanding the full dynamics of environmental exposure in public health research. Nemati et al. [30] reviewed the applications of mobile sensing with smartphones for environmental, transportation and health monitoring. Similar research was also conducted by Aram et al. [31] and Bujari et al. [32], who developed mobile sensing platforms based on smartphones or smartwatches to pervasively collect environmental data. Apte et al. [33], Anjomshoaa et al. [34], Leung et al. [35] and Guo et al. [36] deployed environmental sensors on urban vehicles that routinely navigate through city streets to establish a dynamic network for comprehensive and efficient urban environmental monitoring. Zhou et al. [37], Chen et al. [38] and Guo et al. [39] exploited mobile sensing for the early warning or localisation of gas emissions in a city. These studies cover the shortcomings of traditional ground-based monitoring stations and can lead to further research on the spatio-temporal problems of big data.

For indoor contexts, the mobile sensing idea can retrospect to the use of mobile instrument carts for IEQ monitoring [40]. Traditional IEQ monitoring required a large number of sensors, so researchers developed an instrument cart with multiple sensors to conduct measurements simultaneously at various locations [41–43]. Although this IEQ cart can realize mobile sensing to some extent, it generally relies on considerable labor costs and manual navigation. This drawback hampers automatic continuous monitoring in the long term and limits widespread

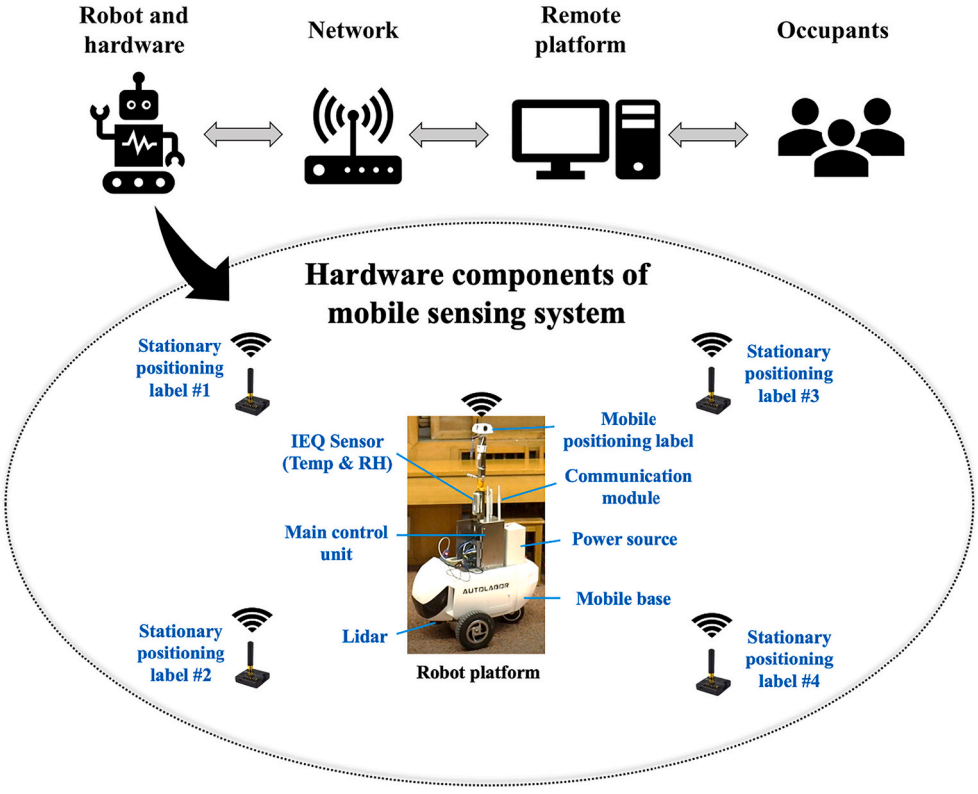

Fig. 1. Architecture and components of the mobile sensing system.

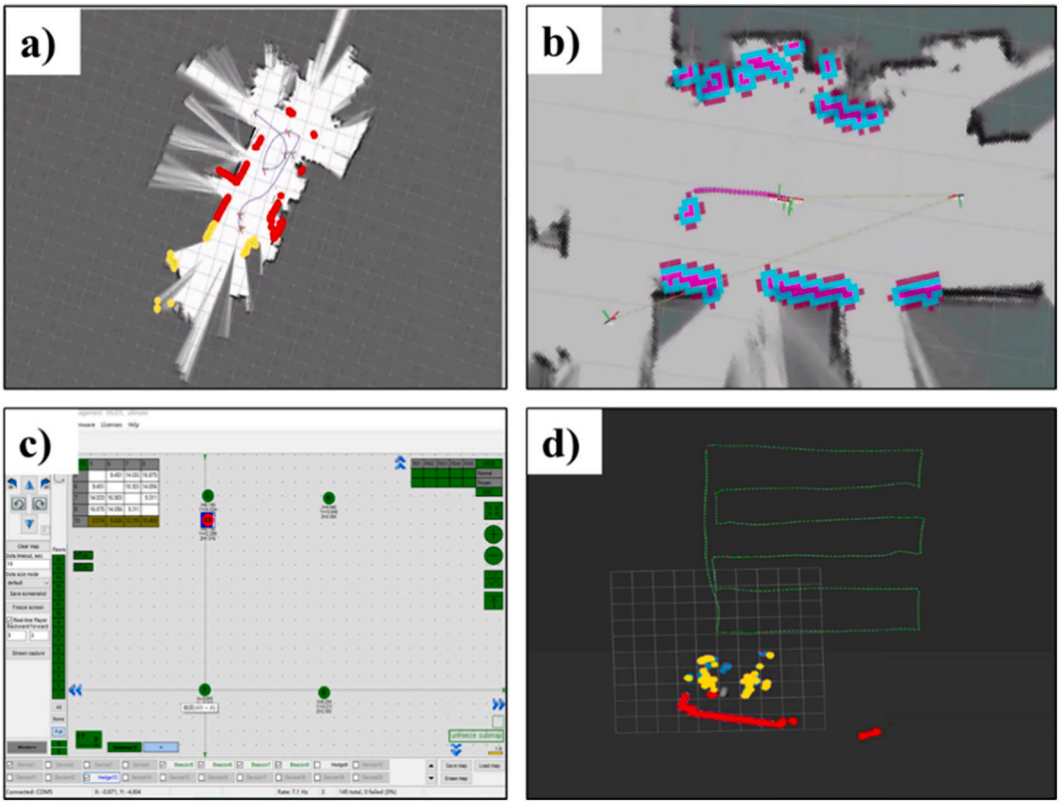

Fig. 2. Snapshots of simultaneous localization and mapping (SLAM) and trajectory tracking technologies: (a) Incrementally built 2-D map from lidar points; (b) Real-time navigation based on SLAM; (c) Setup of the Marvelmind indoor navigation system; (d) Pre-record of moving trajectory.

applications in more buildings.

Today, with the rapid development of robotic technologies and the proliferation of various service robots in the built environment [44], IEQ mobile sensing can be achieved in a more efficient and automated way. Several studies have begun to explore the potential of using building robots for IEQ monitoring [45–50]. For instance, Jin et al. [45], Yang et al. [46], Qian et al. [47] and Wu et al. [48] respectively have proposed an automated mobile sensing system using a robot equipped with IEQ sensors, as well as the corresponding spatio-temporal data processing algorithm. These mobile sensing methods were all examined via real-world experiments and some were also compared with stationary sensing methods. The results showed that robotic mobile sensing can enable the accurate and comprehensive understanding of IEQ spatio-temporal distribution and prompt positioning of contaminant sources. Hu et al. [49,50], who continued to improve the mobile sensing system from a single robot to multiple robots, achieved the cooperation of robots by distributed deep reinforcement learning. This progress means that the robotic mobile sensing system can monitor IEQ more efficiently in a larger space.

Although the above researchers have made preliminary explorations into the mobile sensing of IEQ, two unresolved problems still exist. Firstly, how fast the robot should move is unclear, since the speed requires a trade-off with the sensor response time. If the robot's moving velocity is too high, the measured IEQ data may be inaccurate in some places, because the robot may leave before the IEQ sensor readings have become stabilized. If the robot moves too slowly to ensure enough IEQ sensor response time at each location, the sensing time of global space will become too long, which would be detrimental to the spatio-temporal processing of IEQ data. The appropriate moving velocity for IEQ mobile sensing therefore must be found. Secondly, previous studies have mostly incorporated mobile sensing to replace stationary sensing without effectively integrating the two methods. The mobile and stationary sensing methods both have their plusses and minuses. The mobile sensing method can obtain IEQ maps with better spatial resolution, but this is just a short-term solution because the robot cannot run continuously in the long term. Stationary sensing is the most reliable and convenient method for long-term IEQ monitoring, though the spatial resolution is usually far from satisfactory. An unresolved challenge is how best to combine the mobile and stationary sensing methods so that their respective advantages will be complementary, especially in long-term monitoring.

1.3. Objective

In this paper, air temperature (one of the most significant IEQ parameters) is selected as the monitoring target. A robot-based mobile sensing system for high-resolution temperature monitoring will be developed. Three key questions are expected to be answered:

- What is the effect of robot moving velocity on temperature mobile sensing results?
- What is the short-term solution to obtaining high-resolution thermal maps based on the mobile sensing data?
- How should the mobile and stationary sensing methods work together to achieve long-term monitoring of the thermal environment with suitably high granularity?

2. Robot-based mobile sensing system

2.1. Robot platform

Fig. 1 describes the whole architecture of the mobile temperature sensing system. This study employs Autolabor PM1, an open-source multi-purpose robotic product, as the robotic platform for mobile sensing (http://www.autolabor.com.cn). The speed of the mobile base can be continuously adjusted within the range of 0– 1 m/s, which is

Table 1
Typical information of the air temperature sensor.

Parameter	Range	Resolution	Uncertainty	Minimum data recording interval
Temperature	−40–100 °C	0.1 °C	± 0.3 °C	2 s

sufficient for most indoor mobile sensing tasks. The robot supports remote control in real applications.

The robot operating system (ROS) is a software framework for robot program development. The main control unit of the robot is equipped with an Ubuntu 18.04 system based on ROS. The system has several built-in programs for positioning and navigation; other programs can also be written to meet the special needs of mobile sensing.

2.2. Positioning and navigation system

The robot is equipped with two Faselase D10 2-D lidars using a Simultaneous Localization and Mapping (SLAM) algorithm. SLAM is a technique that simultaneously maps the surrounding environment and calculates the robot's position (Fig. 2a) [51]. The robot can achieve localization and autonomous navigation based on the constructed map (Fig. 2b).

An ultrasonic indoor navigation system (Marvelmind Beacon HW v4.9) was also applied to provide more precise (± 2 cm) location data. The navigation system consists of one mobile label on the robot and several stationary positioning labels distributed on the boundary of the space (Fig. 2c). The mobile beacon's location is calculated based on a propagation delay of ultrasonic pulses between stationary and mobile beacons using the trilateration algorithm.

Based on the above system, the robot can automatically track a pre-recorded trajectory (the green polyline in Fig. 2d). Simultaneously, the real-time coordinates of the robot are recorded.

2.3. IEQ sensor

Air temperature is chosen as the monitoring target because it is a common indicator in thermal comfort research and significantly affects human health and productivity [5–7]. Indoor air temperature also relates to the cooling or heating load of HVAC systems, as well as control performance [12]. The air temperature sensor used in this study is the WSZY-1 sensor, with the typical information presented in Table 1. The sensor has a wide measuring range and high precision. More importantly, the sensor has a short recording interval to collect dense readings along the moving route. All sensors were calibrated before the experiments.

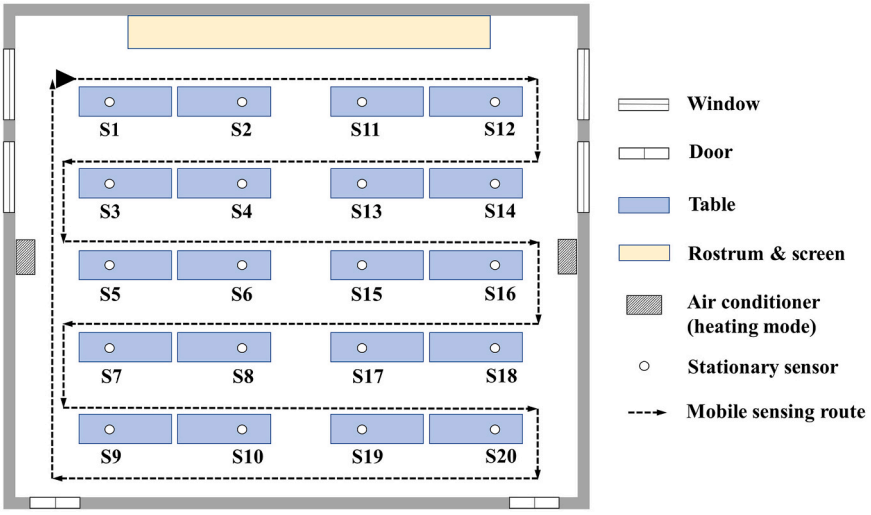

Fig. 3. Floorplan of the experimental space, showing the windows, doors, tables, rostrum, air conditioners, stationary sensors and mobile sensing route.

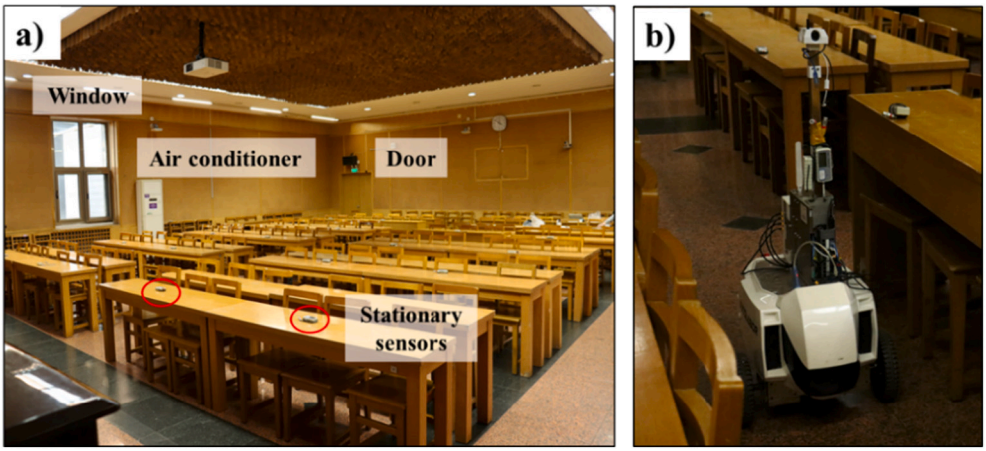

Fig. 4. Snapshots of the experimental site.

Table 2
Robot moving velocity for each experiment.

Experiment no.	Robot moving velocity (m/s)	Rough lap time (min)
I	0.60–0.80	2
II	0.25–0.45	5
III	0.10–0.20	10

3. Experimental setup

3.1. Overview

The objective of experiment is to examine how the mobile sensing method performs while monitoring dynamic inhomogeneous indoor air temperature fields under different conditions. The experiment was conducted in a typical classroom on a winter day in December 2021. The 2-D size of this classroom is 9.6 m (X) * 14.0 m (Y), with a total floor area of 134.4 m^2. Fig. 3 and Fig. 4 show the spatial layout and snapshots of the classrooms.

The classroom has four windows in front and two doors in the back. During the experiments, if we wanted to cool the room, the windows and doors could be opened to provide cold air from outside. Air conditioners are located on the left and right sides of the classroom as heat sources. The maximum heating power is 950 W for each air conditioner. Three experimenters were also present at random positions in the classroom to simulate disturbances in real scenarios.

3.2. Stationary sensors and locations

As shown in Fig. 3, 20 stationary sensors were evenly distributed throughout the classroom. The sensors were all placed at the desks at a height of 0.75 m. The stationary sensors were the same type of sensor as the one on the mobile sensing robot, and they were all calibrated to avoid reading differences between different sensors.

This number of stationary sensor nodes was sufficient in the present study to provide a dense sensing network, and the measured data from each sensor node could roughly represent the air temperature within a square area of 2.5 m * 2.5 m. It should be noted that such a large number of sensors would not normally be deployed during actual measurements. The purpose of this deployment was to obtain the ground truth of indoor air temperature distribution characteristics; the ground truth was further used for comparison with the mobile sensing results.

3.3. Moving route and velocity

The mobile robot measured air temperature during continuous movements without stopping. The dashed line with an arrow in Fig. 3 illustrates the robot's pre-planned moving route. The robot started moving at the front left of the classroom, then went throughout the entire space along the comb-tooth-shaped path before finally returning to the starting point after finishing one lap. The whole trajectory of one lap was about 85 m. During the experiment, multiple laps were repeated in the same manner described above.

The velocity of the robot is one of the main focuses of this study. In order to determine the optimal velocity for mobile sensing, three velocity conditions were designed for comparison (Table 2) to consider the sensor response time and the appropriate lap time. Considering the uncertainty around the preset velocity because of movement component errors and relative navigation algorithms, "velocity ranges" was used instead of "values". For each preset velocity within one velocity range, the actual velocity the robot followed was similar in the real environment, as were the lap time and mobile sensing results. During the high-velocity experiment, the robot moved at a speed range of 0.60–0.80 m/s, or roughly 2 min per lap. During the medium-velocity experiment, the robot moved at a speed range of 0.25–0.45 m/s, or about 5 min per lap. In the low-velocity experiment, the robot moved at a speed range of 0.10–0.20 m/s, or roughly 10 min per lap.

Fig. 5 illustrates the actual trace as the robot moved throughout the space continuously; experiment II is shown as an example. Each dot represents the position of the robot when the air temperature sensor made records at 2-s intervals. In experiment II (0.25–0.45 m/s), the distance between adjacent dots was thus approximately 0.6 m.

3.4. Experimental procedure and conditions

The experiment was carried out in three parts, with each part corresponding to one mobile sensing velocity level. During each sub-experiment, both stationary sensing and mobile sensing were involved simultaneously. The mobile robot continued moving for multiple laps to collect data. Fig. 6 presents the total number of laps in each sub-experiment, as well as the start and end times.

To make the experimental conclusion as comprehensive as possible, complex thermal conditions (which were temporally dynamic and spatially inhomogeneous) were created by changing the status of the air conditioners and doors in a random way. Fig. 6 lists the detailed conditions during each lap. For example, in experiment I (0.60–0.80 m/s),

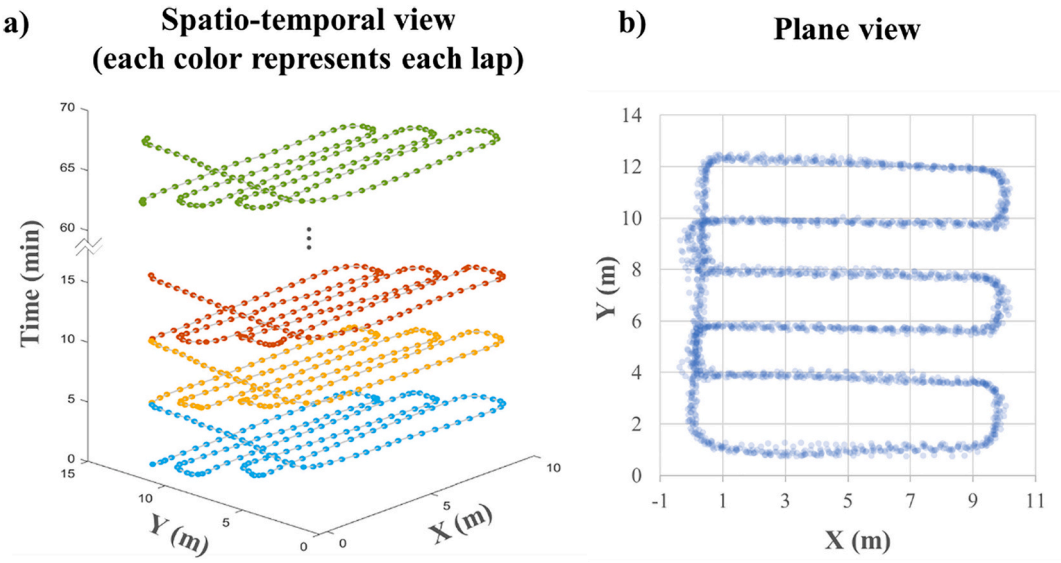

Fig. 5. Actual trace of the robot at 2-s intervals (experiment II, 0.25– 0.45 m/s): (a) Spatio-temporal view; (b) Plane view.

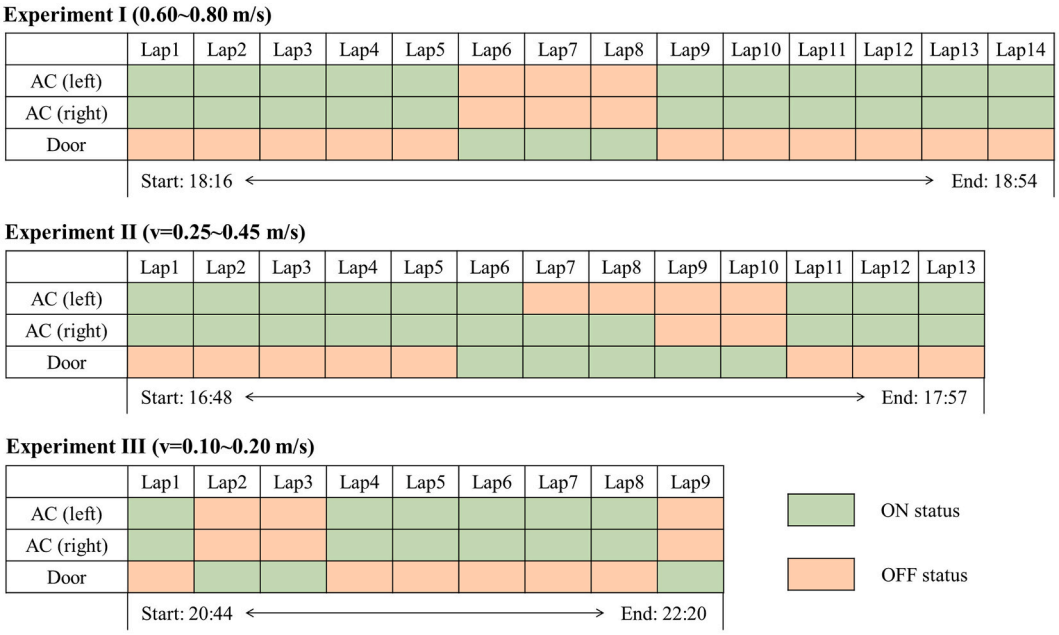

Fig. 6. Experimental conditions for air conditioners and door status during each lap.

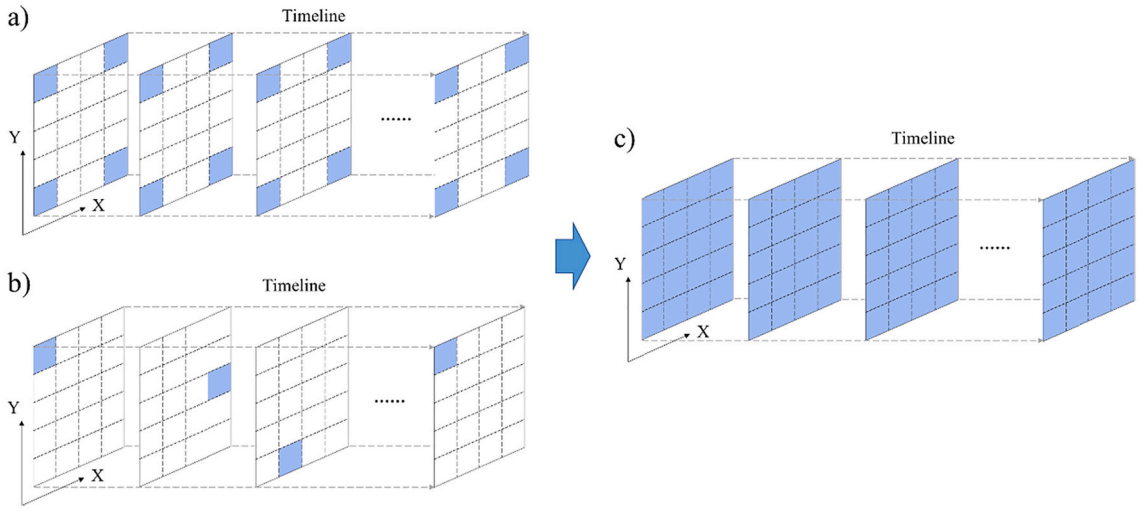

Fig. 7. Illustration of data structures in both the spatial and temporal domains for (a) raw data from stationary sensing; (b) raw data from mobile sensing; (c) targeted data after processing.

the two air conditioners were kept running in heating mode and the doors were closed for laps 1–5 and 9–14, while the two air conditioners were turned off and the doors were open for laps 6–8.

4. Spatio-temporal processing method

The spatio-temporal processing of raw data is an important step in obtaining high-resolution, real-time temperature maps. Fig. 7 provides a vivid illustration of the temperature data structure in both the spatial and temporal domains. Compared with deploying multiple stationary sensors, measurement from one mobile sensor covers the whole space with a higher granularity, although, as shown in Fig. 7b, the data structure for mobile sensing is still sparse in the spatio-temporal domain. In our experiments, for each timestamp, only one location was monitored and the other 19 were unknown; for each location, the back-to-back monitoring interval was rather long, equalling the lap time of the robot (2– 10 min). Therefore, scientific spatio-temporal processing methods were required to complement data blanks in both the spatial and temporal domains to achieve the targeted data structure, as shown in Fig. 7c.

Sections 4.1 and 4.2 further illustrate the detailed spatio-temporal processing solutions in the short term (only by mobile sensing) and long term (by the cooperation of mobile and stationary sensing), respectively. After completing the spatio-temporal data of 20 locations, the spatial interpolation method was adopted to generate 2-D heat maps for better visualization. Since interpolation is only a means to improve the visual effects and is not the focus of this paper, the classic method of triangulation with cubic interpolation was adopted. The method is exact and involves a small computing load and is often used to conduct quick interpolation from sparse data on regularly spaced samples [52]. The interpolation function code is available off the shelf in MATLAB.

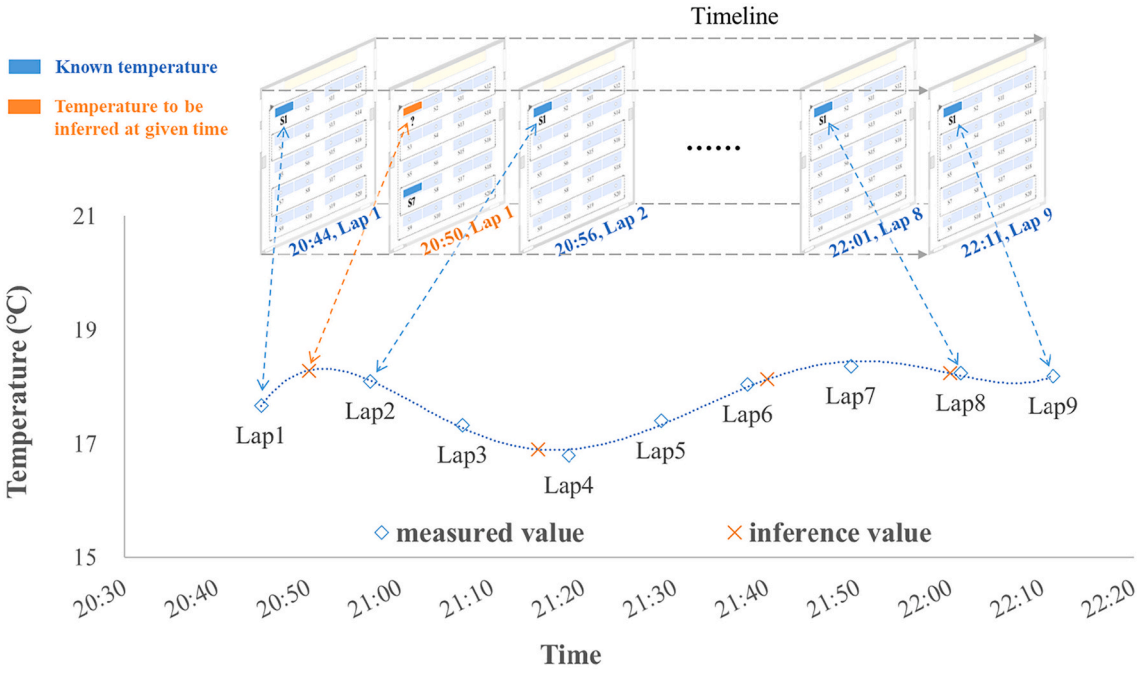

Fig. 8. Schematic diagram of the time-series trend fitting method at a certain location (experiment III, 0.10– 0.20 m/s, S1 position).

4.1. Short-term solution by mobile sensing

The mobile sensing data alone is sufficient to fill in spatio-temporal data blanks in the short term. The robot moves repeatedly in the space along the preset trajectory, gathering multiple air temperature samples for each location. In our experiments, the interval of adjacent samples for each location was 2, 5 and 10 min (i.e. the time the robot took to finish a lap). The time-series trend fitting method can be used to infer the unknown air temperatures at other time stamps between the two adjacent visits of robot to the same location. For better illustration, Fig. 8 further shows the basic idea of time-series trend fitting, using the location S1 in experiment III as an example. During the 90-min experiment, S1 was directly measured nine times at 10-min intervals. The nine samples were then used to fit the air temperature variation curve of S1 during the whole period. With the fitting curve, the temperature of S1 at any time could be inferred: for example, at 20:50, when the robot was away from S1. The above steps were repeated for the data processing of the other 19 locations.

Specifically, for any location i, the non-linear time-series fitting curve $\widehat{f}(t)$ can be solved analytically based on the polynomial function, given by:

$$\widehat{f}(t) = a_0 + a_1 t + a_2 t^2 + \cdots + a_n t^n \tag{1}$$

where t is the timestamp and a_0,a_1,⋯,$a_n$are parameters to be determined by the ordinary least squares (OLS), given by:

$$(a_0, a_1, \cdots, a_n) = argmin \sum_{j=1}^{m} \left(y_{t_j} - \widehat{f}(t_j) \right)^2 \tag{2}$$

where y_{t_j} represents the mobile sensing sample of location i at timestamp t_j in lap j, and m is the total number of samples of location i. The highest order of polynomials, n, is determined by the number of times the thermal environment changes at first. For example, in experiment III, the status of air conditioners and door was switched four times, which indicate n should be fifth. Furthermore, n should be less than the number of samples, m, so that function (2) can have a solution.

There are two main reasons for selecting the polynomial function. Firstly, indoor air temperature usually does not fluctuate frequently in the short term and the number of increase or decrease is countable. Secondly, the sampling interval in our experiments is dense (from 2 min to 10 min), which guarantees the air temperature variation between two samples is small. Therefore, the polynomial function, although simple, is sufficient for the curve fitting.

4.2. Long-term solution by the cooperation of mobile and stationary sensing

The mobile sensing data itself is insufficient for obtaining real-time air temperature maps in the long term because the robot cannot run incessantly in practice. Stationary sensing can take over the task once mobile sensing is absent. In this way, a long-term solution is divided into two situations, depending on whether mobile sensing is present or absent.

Firstly, mobile sensing was used to form a preliminary understanding of the whole environment and to accumulate original data in the short term. The robot was present during this period and the time-series trend fitting method was used for data processing (the same as in Section 4.1). Afterwards, the mobile sensing data was further analyzed to select several representative locations for the deployment of stationary sensors in the next step. Air temperature spatial correlation models from representative locations to other locations were also trained in this step.

Secondly, when the robot was absent, several stationary sensors were deployed at the representative locations mentioned above. The collected stationary sensing data was then input into the spatial models learned from the mobile sensing dataset to infer real-time temperatures at all other locations. With the above method, high-granularity air temperature maps could be obtained even if mobile sensing is absent.

It should be noted that the above two steps alternated in sequence, such as in a relay race. Rather than the cycle occurring only once, it repeated multiple times in the long term. The dataset was constantly accumulating and updating for the selection of representative locations, and for the model training for spatial relationships among all locations.

In the long-term solution, the key challenges were the determination of representative locations and the establishment of the spatial correlation models. For the selection of representative locations, the Pearson correlation coefficient was calculated, which is a commonly used metric to indicate the similarity between variables or vectors. The coefficient

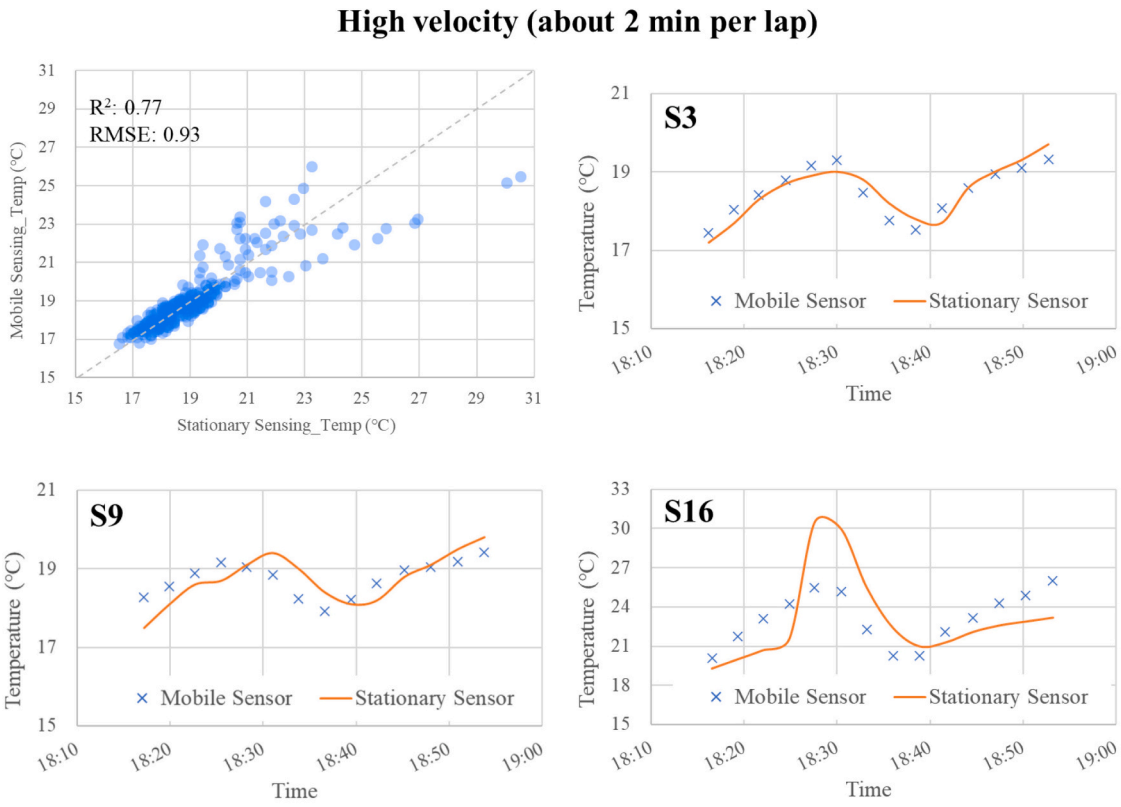

Fig. 9. Comparisons between stationary sensing (ground truth) and mobile sensing with different moving velocities.

between two certain locations A and B is given by:

$$r(A,B) = \frac{n\cdot\sum_{i=1}^{n} a_i\cdot b_i - \sum_{i=1}^{n} a_i\cdot\sum_{i=1}^{n} b_i}{\sqrt{n\cdot\sum_{i=1}^{n} a_i^2 - \left(\sum_{i=1}^{n} a_i\right)^2}\cdot\sqrt{n\cdot\sum_{i=1}^{n} b_i^2 - \left(\sum_{i=1}^{n} b_i\right)^2}} \quad (4)$$

where a and b are the air temperature data at location A and B, and n is the total number of samples at each location. If several locations have high Pearson correlation coefficients with each other, they share strong similarities in temperature variation. In this way, 20 locations were divided into several similar divisions, and representative locations were picked from each division.

For the model development, a variety of data-driven algorithms were implemented to capture the underlying quantitative relationship among the temperatures at different locations, including linear regression (LR), lasso regression, K-nearest neighbour (KNN), support vector regression (SVR), decision tree (DT) and random forest (RF).

LR assumes that the correlation between input and output variables is linear. Lasso regression introduces a regularization term in the loss function to avoid overfitting in LR. KNN is a machine learning algorithm that predicts the unknown according to its neighbours in the feature space. The other three algorithms (SVR, DT and RF) are used to capture nonlinear relationships among variables, which can exist in a temperature field because of the delayed response to heat source changes. SVR searches for optimal strip-like margins to cover as many samples as possible and introduces a kernel function to handle nonlinear relationships. DT divides the feature space by a series of binary nodes, with a specific output for each sub-space. RF adopts DT as the basic model, and the prediction result is a synthesis of all basic models.

The model development was implemented in Python using the scikit-learn library. The model inputs were temperature at the selected representative locations, and the outputs were temperature at the other locations. The whole dataset used for model development was divided into a training set and a validation set at a ratio of 4:1. Parameter optimisation was conducted during each training process.

5. Results and discussion

5.1. Effect of robot moving velocity on mobile sensing accuracy

The moving velocity influences the accuracy of mobile sensing, as mentioned in Section 1.2. Due to the response time of the sensor, the parameter being measured takes time to stabilize at each location. An overly fast velocity thus results in an inevitable deviation from the real value.

To determine the appropriate velocity range for accurate mobile sensing, the mobile sensing data under different velocities were compared with the stationary sensing (ground truth) results, as shown in Fig. 9. The blue scatter plot (where the horizontal axis shows stationary sensing data and the vertical axis shows mobile sensing data) illustrates the comparative results of all measured locations. S3, S9 and S16 were chosen as examples to compare the stationary and mobile sensing data in temporal variation curves. R-square and root mean square error (RMSE) values between stationary and mobile sensing were also calculated.

When the robot moved at 0.25–0.45 m/s and 0.10–0.20 m/s, the stationary and mobile sensing data were fairly consistent, with R-squares of 0.94 and 0.86, respectively, and the scattered points were mainly distributed near the diagonal. The RMSE values were also small (0.73 and 0.68, respectively). When the robot moved at high velocity, however, the mobile sensing data significantly deviated from the ground truth, with a lower R-square (0.77) and a higher RMSE (0.93) value. Obvious phase delays and extreme values also occurred in the time series compared with the ground truth, especially at S9 and S16.

Based on the above comparisons, the high velocity of 0.60–0.80 m/s was too fast to collect accurate temperature data, while 0.25–0.45 m/s

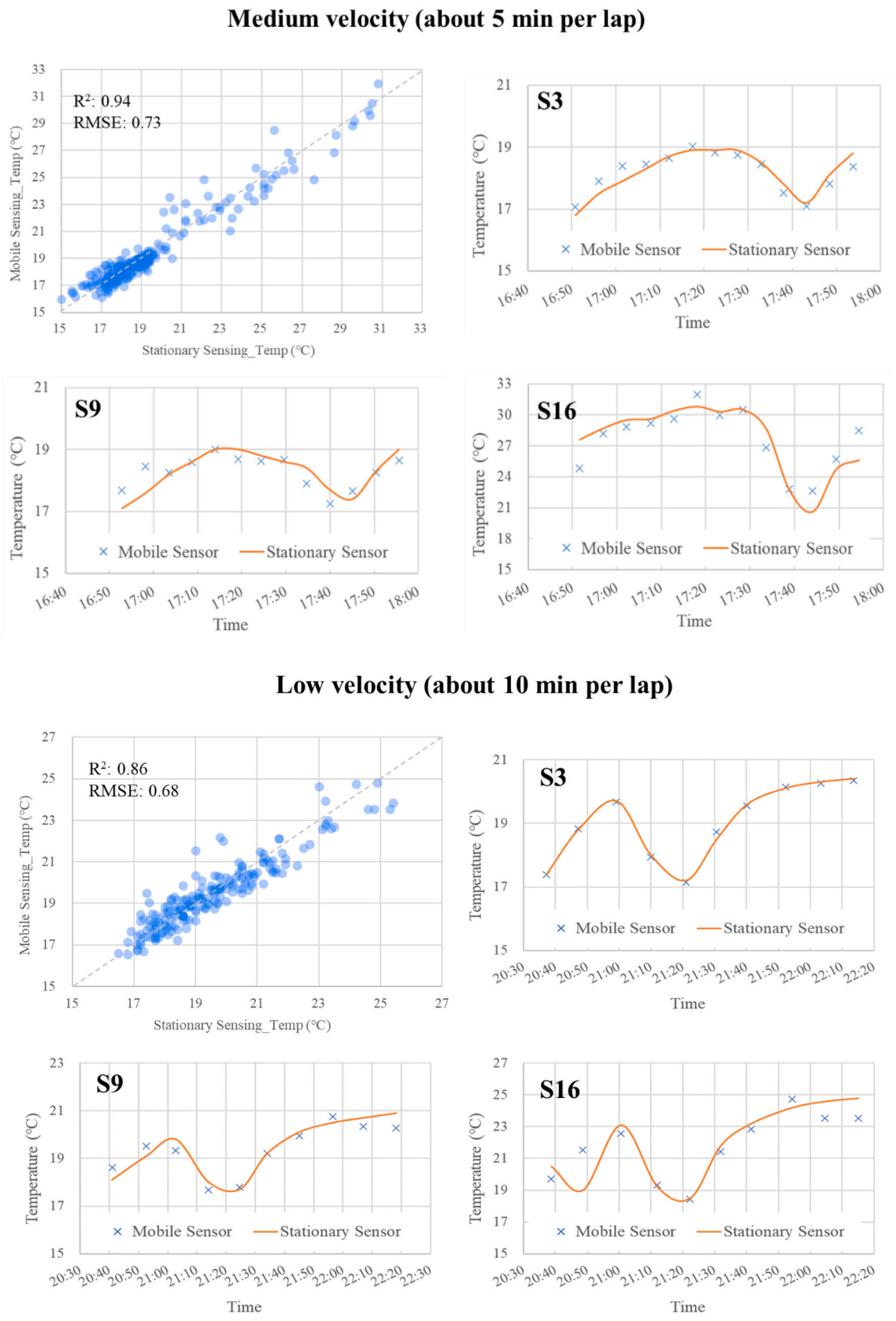

Fig. 9. (*continued*).

and 0.10–0.20 m/s were appropriate for the measurement stage. It should be noted that this result is not a universal conclusion. The appropriate range of velocity may vary with different heat source conditions, moving trajectories and sensor properties. If the mobile sensing is introduced into an unfamiliar environment, preliminary experiment should be conducted to determine the appropriate moving

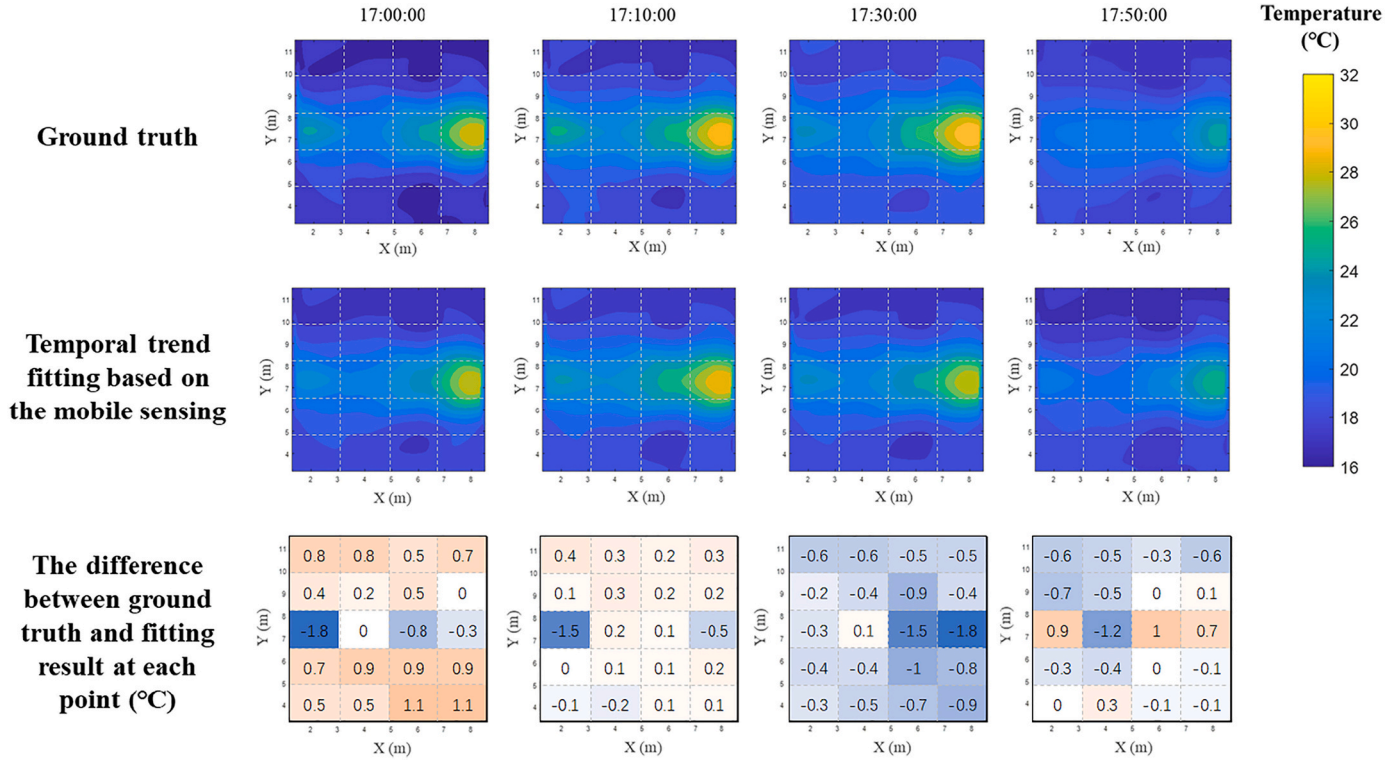

Fig. 10. Air temperature maps derived from mobile sensing using the time-series trend fitting method and comparisons with the ground truth (experiment II, 0.25–0.45 m/s).

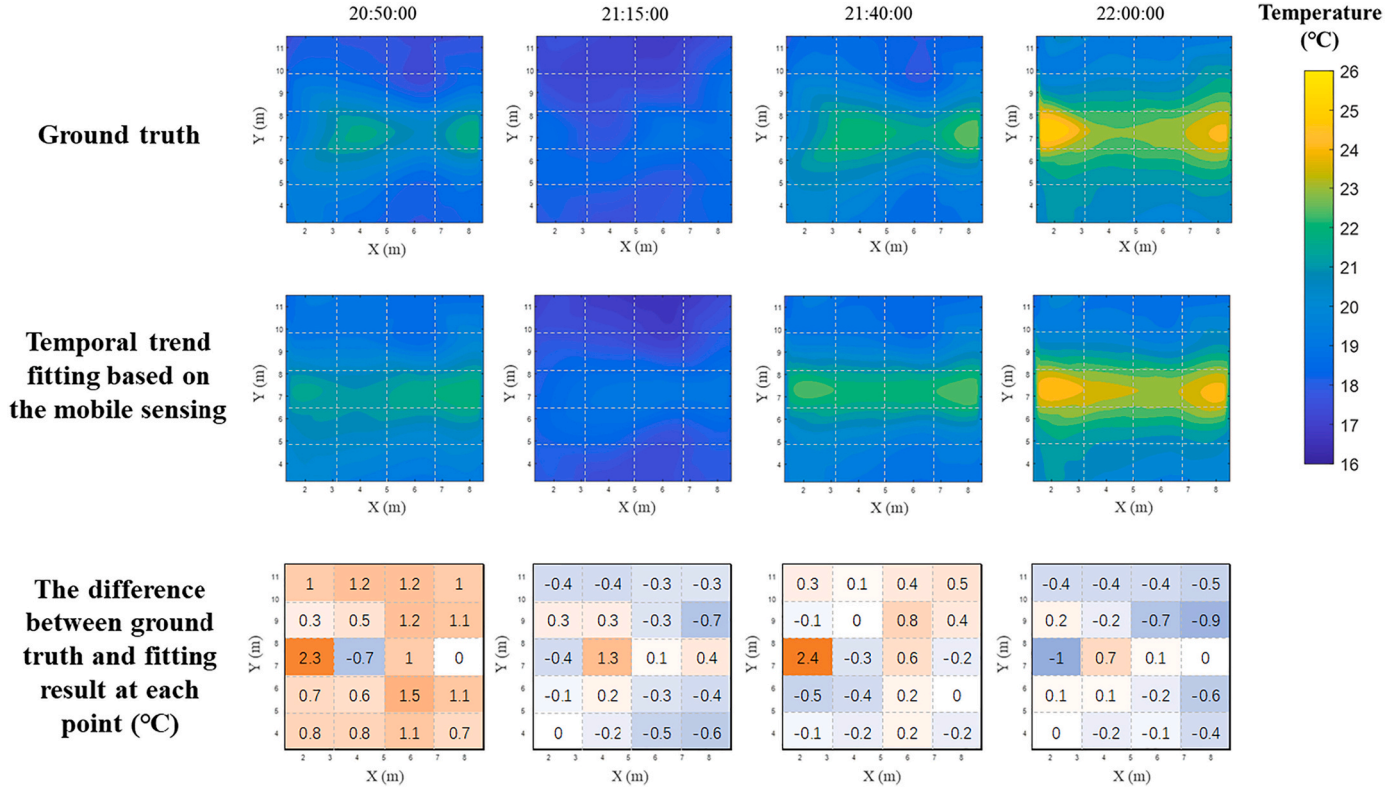

Fig. 11. Air temperature maps derived from mobile sensing using the time-series trend fitting method and comparisons with the ground truth (experiment III, 0.10–0.20 m/s).

Table 3
List of locations with an absolute difference between estimated temperature and ground truth larger than 1.0 °C and 2.0 °C, respectively (experiments II and III).

Experiment no.	Location list (deviation >1.0 °C)	Location list (deviation >2.0 °C)
II (0.25–0.45 m/s)	S5, S6, S15, S16, S19, S20 (6 locations)	None
III (0.10–0.20 m/s)	S2, S5, S6, S11, S13, S14, S17, S18, S19 (9 locations)	S5 (1 location)

Table 4
RMSE and correlation coefficients between the mobile sensing estimation and ground truth in the whole space (experiments II and III).

Experiment no.	RMSE	Correlation coefficient
II (0.25–0.45 m/s)	0.64	0.98
III (0.10–0.20 m/s)	0.69	0.92

velocity.

This section has addressed the issue of mobile sensing velocity from the measurement stage. The next section will further explore how the medium and low velocities affected the data processing stage and final accuracy.

5.2. Short-term temperature distribution estimated by mobile sensing

The 20 stationary sensors were used as the ground truth to verify the reliability of the data processing method in the short term. Both experiments II (0.25– 0.45 m/s) and III (0.10– 0.20 m/s) were analyzed to see how robot velocity affected the performance of the time-series trend fitting method, as shown in Fig. 10 and Fig. 11. The spatial distribution characteristics of the temperatures obtained in the experiments were presented in the form of heat maps, which were smoothed by cubic interpolation. Such heat maps can be obtained at any timestamp; four typical timestamps in experiments II and III were chosen as examples.

Other than minor differences in some locations, the spatio-temporal characteristics derived from the time-series trend fitting method were mostly consistent with the ground truth in experiments II and III. To further quantify the accuracy, several indexes of each location and the whole space were calculated. Table 3 lists the locations that had significant estimated deviations (larger than 1.0 °C and 2.0 °C, respectively) in experiments II and III. Furthermore, the data from all locations were taken as a whole; RMSE values and correlation coefficients between the estimation and ground truth were calculated in order to evaluate the comprehensive accuracy (see Table 4).

The above results indicate that the time-series trend fitting method generally performed better at 0.25–0.45 m/s for obtaining more accurate indoor temperature distribution maps. As the velocity decreased from 0.25 to 0.45 m/s to 0.10–0.20 m/s, more locations significantly deviated from the ground truth; the overall indoor temperature estimation had a higher RMSE (from 0.64 to 0.69) and weaker consistency (from 0.98 to 0.92) with the real distribution. One possible reason is that the lower velocity resulted in a longer interval between adjacent samples at each location, thus missing critical temporal variations within the interval.

In conclusion, the time-series trend fitting method was generally sufficient for capturing short-term spatio-temporal characteristics in the whole space. Compared with the low-velocity experiment, 0.25–0.45 m/s was more appropriate for estimating temperature variations with the method.

5.3. Long-term temperature distribution estimated by mobile and stationary sensing

In this section, the long-term solution by the cooperation of mobile and stationary sensing was examined. Firstly, the mobile sensing data in experiment II was used to guide the location selection of stationary sensors in the next period and to train the spatial prediction model. Fig. 12 shows the correlation coefficient matrix among all locations calculated by the mobile sensing data in experiment II. In the matrix, the values at the intersection of certain rows and columns represent the correlation coefficient between the corresponding two locations. A higher correlation coefficient means that the two locations are more similar in temperature characteristics. According to the correlation coefficient matrix, 20 locations in the whole space could be classified into four divisions: division #1 includes S1, S2, S11, S12, S17, S18, S19 and S20; division #2 includes S3, S4 and S13; division #3 includes S5, S6, S14, S15 and S16; and division #4 includes S7, S8, S9 and S10. Within each division, all locations were highly correlated with correlation coefficients >0.8, thereby reducing multiple locations to one representative location. As a result, S3, S9, S15 and S20 were chosen as typical stationary sensing locations in the next period.

The temperatures at these four locations were used as inputs to train

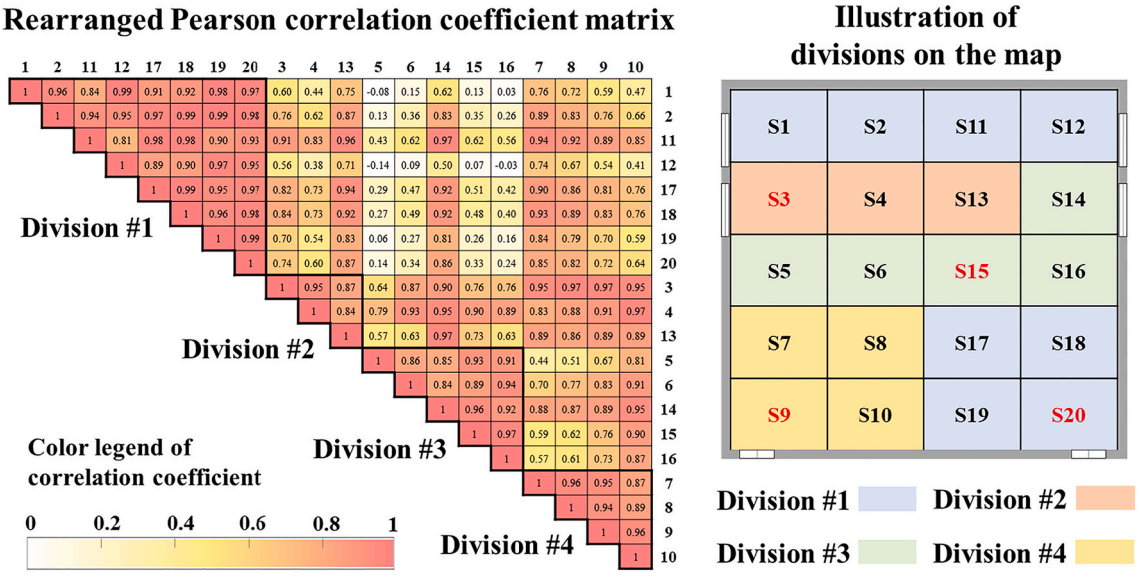

Fig. 12. Pearson correlation coefficient matrix of temperatures at different locations.

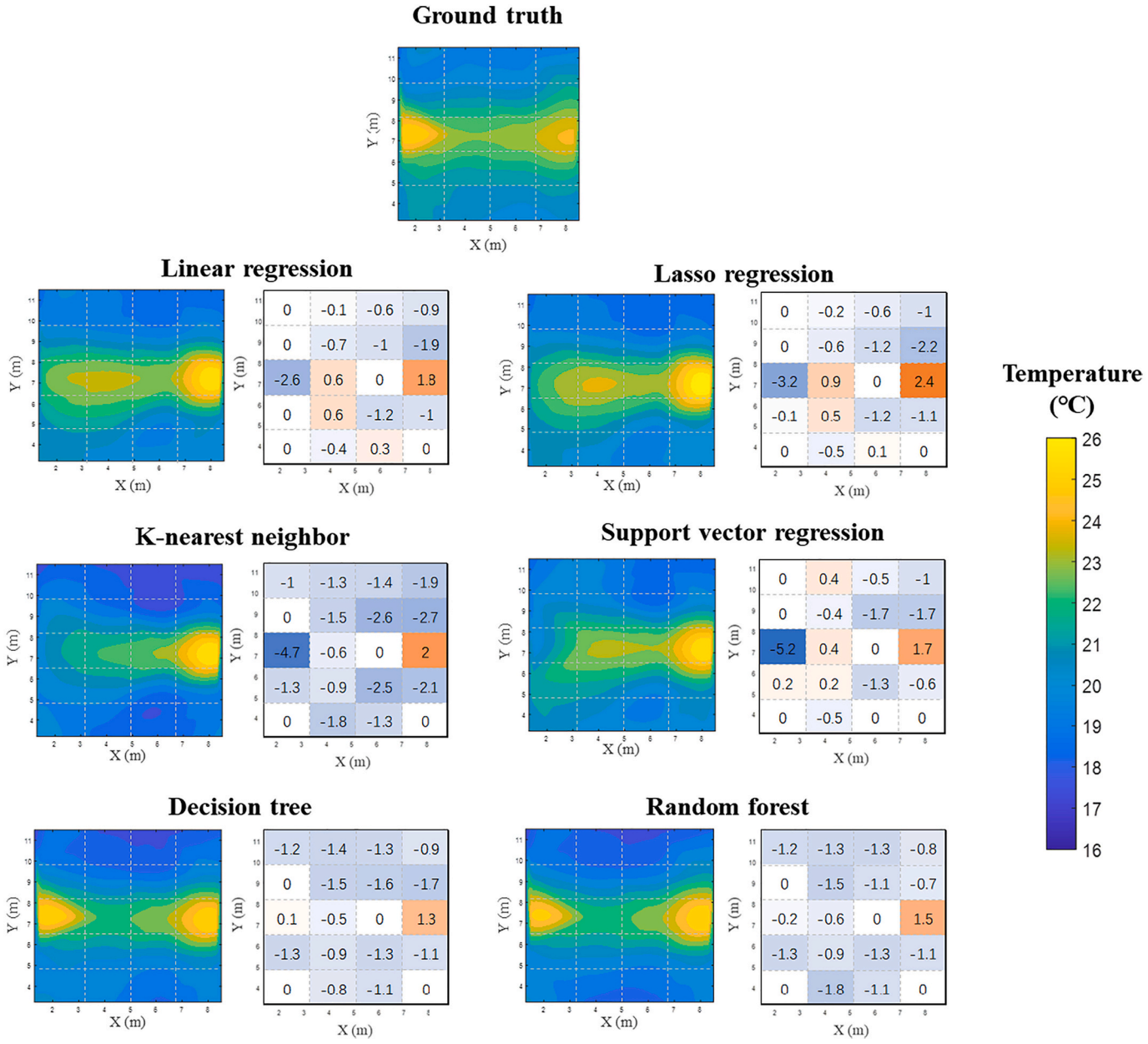

Fig. 13. Prediction results of temperature distribution maps at one representative moment (both air conditioner on, door closed) using different models and stationary sensing data of S3, S9, S15 and S20. The ground truth was generated from all 20 stationary sensors.

Table 5
Comparison results of RMSE for temperature prediction in the entire space and the corresponding Pearson correlation coefficients between the prediction and ground truth during the whole period of experiment III.

Algorithm	RMSE	Correlation coefficient
LR	1.14	0.85
Lasso	1.16	0.80
KNN	1.28	0.84
SVR	0.97	0.87
DT	0.75	0.98
RF	0.68	0.98

the model to predict temperatures at other locations, which could be used to further generate the whole temperature distribution map. According to the description found in Section 4.2, six models (LR, lasso, KNN, SVR, DT and RF) were used, and their prediction performances were compared in the next period.

Subsequently, it was assumed that experiment III was a period without mobile sensing (despite the fact that the mobile sensing experiment was present) and that only data from the stationary sensors at S3, S9, S15 and S20 was available. Under such conditions, the previously trained spatial prediction model and the current stationary sensing data at limited locations were used to generate a whole temperature distribution map in real time. Fig. 13 shows an exemplificative result at a certain moment and compares the predicted temperature maps through different data-mining models. As the figure shows, the temperature distribution characteristics predicted by the decision tree and random forest methods were relatively consistent with the ground truth, while other data-mining models failed to accurately identify the occurrence of the left heat source.

For further comparison, Table 5 lists the RMSE values for temperature prediction in the entire space as well as the correlation coefficients between the prediction and ground truth during the whole period of

experiment III (test set). Since the typical values of air temperature were around 20 °C, the reduction of RMSE from 1.28 (KNN) to 0.68 (RF) was significant from a practical point of view. RF performed best at depicting the temperature distribution among the six algorithms selected. RF also had the highest correlation coefficient of 0.98, which outperformed other algorithms such as lasso regression (0.80). This finding indicated that RF's temperature prediction at unknown points followed a more similar trend to the ground truth.

5.4. Potential applications

Mobile sensing serves as a low-cost, high-resolution environmental monitoring solution in large spaces. For large-scale spaces such as airport terminals and shopping malls, one robot can replace tens or even hundreds of fixed sensors to achieve the same spatial high resolution, resulting in a major reduction in investment and maintenance expenses. Environmental controls can also be improved with high-resolution data.

Because fixed sensors are always constrained by installation locations such as walls and columns, stationary sensing usually fails to monitor environment parameters in the middle of large spaces (e.g. between the seats of an airport terminal waiting area) without available installation locations. In contrast, robots, as mobile installation platforms for sensors, can move freely through the centre of the space. Many hidden environmental problems can be detected with this strong spatial accessibility.

Mobile sensing systems are capable of actively tracking environmental problems. Environmental anomalies in large spaces (e.g. cold wind infiltration from windows, or air pollutants exhaled by a smoker) can be sparsely distributed and can fluctuate dramatically. Mobile sensing can quickly trace source cues based on airflow or concentration information [53], even if the source keeps moving.

5.5. Limitations

The proposed mobile sensing system still has several limitations before it can be used for real-world environmental monitoring.

Firstly, the time-series fitting method could be further optimised. Although the polynomial function is generally adequate for most short-term scenarios, large fitting deviations may occur in some extreme conditions with rapid and drastic temperature fluctuations. Under such circumstances, more intensive sampling is required. Furthermore, the whole time-series data may need to be split into several parts to conduct the regression separately.

Secondly, the mobile sensing performances of other IEQ parameters (such as CO_2, $PM_{2.5}$, illuminance, etc.) have not been tested. The proposed mobile sensing process should be adjusted for other IEQ parameters because of the differences in mechanisms and measurement methods. For example, the dispersion mechanism of air pollutants is more complex than air temperature. Problems may also occur if multiple IEQ parameters are measured simultaneously. Because optimal trajectories and velocities may vary with different IEQ parameters, the basic settings of the mobile sensing system require careful trade-offs.

Thirdly, human disturbances were not considered in the experiment. Moving occupants can cause occasional disturbances if they pass through the preset trajectory and interrupt the mission. The adopted robot platform is equipped with an obstacle avoidance algorithm to bypass the obstacle and return to the trajectory automatically. In an overcrowded space, however, the robot frequently performs obstacle avoidance and path planning, both of which significantly delay the mobile sensing mission. Investigations into people densities and activity patterns will be necessary before the mobile sensing system may be deployed in real-life scenarios.

Fourthly, the impact of battery endurance on mobile sensing should be addressed. In our experiment, the battery capacity was sufficient to power the robot to run dozens of laps in the classroom. However, as space becomes larger, the energy consumption of robot may increase dramatically, which limits the popularization and application of mobile sensing.

6. Conclusions

This paper describes a robot-based mobile sensing system for high-resolution temperature monitoring. The integrated system mainly consists of a mobile robot base, a positioning system and an air temperature sensor. A series of experiments in a classroom setting were conducted to test the air temperature measurements from the mobile sensing system by making comparisons with the dense stationary sensor network. According to the experimental results, 0.25– 0.45 m/s (medium velocity) was the optimal speed of the robot for high-resolution indoor temperature monitoring, compared to 0.60– 0.80 m/s (high velocity) and 0.10–0.20 m/s (low velocity).

Spatio-temporal processing methods were developed to reconstruct continuous thermal maps from the data collected in the experiments, which was sparse in both the spatial and temporal domains. For short-term monitoring, mobile sensing was sufficient to capture the spatio-temporal characteristics in the whole space, based on the time-series trend fitting method. For long-term monitoring, a small number of stationary sensors and a spatial prediction model were introduced to cooperate with the mobile sensing, which is capable of continuously generating high-granularity thermal maps even if mobile sensing is absent. Among the many data-mining algorithms used in this paper, random forest was found to perform best for the establishment of the spatial prediction model. In conclusion, the mobile sensing system can assess and diagnose indoor temperatures with high spatial granularity and accuracy, as long as the robot velocity and data processing method are well planned for addressing specific problems.

Future work will be conducted to include more IEQ parameters and to extend the potential applications of the mobile sensing system. A clearer and more comprehensive understanding of the indoor environment can be formed by using the high-resolution spatio-temporal distributions of various parameters. The mobile sensing system is also expected to interact with the automatic building control system. Using this approach, building researchers can further reduce sensing costs, improve building operation efficiency and achieve intelligent decision-making.

Declaration of Competing Interest

The authors declare that they have no known competing financial interests or personal relationships that could have appeared to influence the work reported in this paper.

Acknowledgments

This study is supported by the National Natural Science Foundation of China (Grant No. 52130803, 51825802, 51521005). The first author acknowledges the China Postdoctoral Science Foundation (Grant No. 2021M691789).

References

[1] Y. Geng, W. Ji, Z. Wang, B. Lin, Y. Zhu, A review of operating performance in green buildings: energy use, indoor environmental quality and occupant satisfaction, Energy Build. 183 (2019) 500–514, https://doi.org/10.1016/j.enbuild.2018.11.017.

[2] P. Li, Y. Lu, D. Yan, J. Xiao, H. Wu, Scientometric mapping of smart building research: towards a framework of human-cyber-physical system (HCPS), Autom. Constr. 129 (2021), 103776, https://doi.org/10.1016/j.autcon.2021.103776.

[3] J. Al Dakheel, C. Del Pero, N. Aste, F. Leonforte, Smart buildings features and key performance indicators: a review, Sustain. Cities Soc. 61 (2020), 102328, https://doi.org/10.1016/j.scs.2020.102328.

[4] M. Jia, A. Komeily, Y. Wang, R.S. Srinivasan, Adopting internet of things for the development of smart buildings: a review of enabling technologies and applications, Autom. Constr. 101 (2019) 111–126, https://doi.org/10.1016/j.autcon.2019.01.023.

[5] O. Jay, A. Capon, P. Berry, C. Broderick, R. de Dear, G. Havenith, Y. Honda, R. S. Kovats, W. Ma, A. Malik, N.B. Morris, L. Nybo, S.I. Seneviratne, J. Vanos, K. L. Ebi, Reducing the health effects of hot weather and heat extremes: from personal cooling strategies to green cities, Lancet 398 (2021) 709–724, https://doi.org/10.1016/S0140-6736(21)01209-5.
[6] Y. Al Horr, M. Arif, M. Katafygiotou, A. Mazroei, A. Kaushik, E. Elsarrag, Impact of indoor environmental quality on occupant well-being and comfort: a review of the literature, international journal of sustainable, Built Environ. 5 (2016) 1–11, https://doi.org/10.1016/j.ijsbe.2016.03.006.
[7] Y. Geng, W. Ji, B. Lin, Y. Zhu, The impact of thermal environment on occupant IEQ perception and productivity, Build. Environ. 121 (2017) 158–167, https://doi.org/10.1016/j.buildenv.2017.05.022.
[8] Y. Liu, Z. Wang, Z. Zhang, J. Hong, B. Lin, Investigation on the indoor environment quality of health care facilities in China, Build. Environ. 141 (2018) 273–287, https://doi.org/10.1016/j.buildenv.2018.05.054.
[9] Z. Pei, B. Lin, Y. Liu, Y. Zhu, Comparative study on the indoor environment quality of green office buildings in China with a long-term field measurement and investigation, Build. Environ. 84 (2015) 80–88, https://doi.org/10.1016/j.buildenv.2014.10.015.
[10] D. Zhuang, X. Zhang, Y. Lu, C. Wang, X. Jin, X. Zhou, X. Shi, A performance data integrated BIM framework for building life-cycle energy efficiency and environmental optimization design, Autom. Constr. 127 (2021), 103712, https://doi.org/10.1016/j.autcon.2021.103712.
[11] H. Kim, T. Hong, J. Kim, Automatic ventilation control algorithm considering the indoor environmental quality factors and occupant ventilation behavior using a logistic regression model, Build. Environ. 153 (2019) 46–59, https://doi.org/10.1016/j.buildenv.2019.02.032.
[12] P. Zhou, G. Huang, Z. Li, Demand-based temperature control of large-scale rooms aided by wireless sensor network: energy saving potential analysis, Energy Build. 68 (2014) 532–540, https://doi.org/10.1016/j.enbuild.2013.10.005.
[13] Building Research Establishment Ltd, Why choose BREEAM?. [WWW Document], URL, https://www.breeam.com/discover/why-choose-breeam/, 2021. accessed 2.11.21.
[14] United States Green Building Council, LEED, v4.1 certification. [WWW Document], URL, https://www.usgbc.org/leed/v41, 2021. accessed 2.11.21.
[15] International WELL Building Institute, WELL, v2 certification. [WWW Document], URL, https://www.wellcertified.com/certification/v2/, 2021. accessed 2.11.21.
[16] ASHRAE/CIBSE/USGBC, Performance Measurement Protocols for Commercial Buildings, ASHRAE Transactions, American Society of Heating, Refrigerating and Air-Conditioning Engineers, January 1, 2010. ISBN-13: 978-1933742793, ISBN-10: 1933742798, 298 pages.
[17] B. Pollard, F. Held, L. Engelen, L. Powell, R. de Dear, Data fusion in buildings: synthesis of high-resolution IEQ and occupant tracking data, Sci. Total Environ. 776 (2021), 146047, https://doi.org/10.1016/j.scitotenv.2021.146047.
[18] W. Zhang, K. Hiyama, S. Kato, Y. Ishida, Building energy simulation considering spatial temperature distribution for nonuniform indoor environment, Build. Environ. 63 (2013) 89–96, https://doi.org/10.1016/j.buildenv.2013.02.007.
[19] T. Ramos, S. Dedesko, J.A. Siegel, J.A. Gilbert, B. Stephens, Spatial and temporal variations in indoor environmental conditions, human occupancy, and operational characteristics in a new hospital building, PLoS One 10 (2015), e0118207, https://doi.org/10.1371/journal.pone.0118207.
[20] J.Y. Lee, P. Wargocki, Y.H. Chan, L. Chen, K.W. Tham, Indoor environmental quality, occupant satisfaction, and acute building-related health symptoms in Green Mark-certified compared with non-certified office buildings, Indoor Air 29 (2019) 112–129, https://doi.org/10.1111/ina.12515.
[21] T. Parkinson, A. Parkinson, R. de Dear, Continuous IEQ monitoring system: context and development, Build. Environ. 149 (2019) 15–25, https://doi.org/10.1016/j.buildenv.2018.12.010.
[22] S. Abraham, X. Li, Design of a low-cost wireless indoor air quality sensor network system, Int. J. Wireless Inf. Networks 23 (2016) 57–65, https://doi.org/10.1007/s10776-016-0299-y.
[23] A.S. Ali, Z. Zanzinger, D. Debose, B. Stephens, Open-Source Building Science Sensors (OSBSS): a low-cost Arduino-based platform for long-term indoor environmental data collection, Build. Environ. 100 (2016) 114–126, https://doi.org/10.1016/j.buildenv.2016.02.010.
[24] Y. Geng, Z. Zhang, J. Yu, H. Chen, H. Zhou, B. Lin, W. Zhuang, An intelligent IEQ monitoring and feedback system: development and applications, Engineering (2021), https://doi.org/10.1016/j.eng.2021.09.017.
[25] Y. Geng, B. Lin, J. Yu, H. Zhou, W. Ji, H. Chen, Z. Zhang, Y. Zhu, Indoor environmental quality of green office buildings in China: large-scale and long-term measurement, Build. Environ. 150 (2019) 266–280, https://doi.org/10.1016/j.buildenv.2019.01.014.
[26] M. Jin, N. Bekiaris-Liberis, K. Weekly, C.J. Spanos, A.M. Bayen, Occupancy detection via environmental sensing, IEEE Trans. Autom. Sci. Eng. 15 (2018) 443–455, https://doi.org/10.1109/TASE.2016.2619720.
[27] A. Bulińska, Z. Popiołek, Z. Buliński, Experimentally validated CFD analysis on sampling region determination of average indoor carbon dioxide concentration in occupied space, Build. Environ. 72 (2014) 319–331, https://doi.org/10.1016/j.buildenv.2013.11.001.
[28] J. Chen, H. Chen, X. Luo, Collecting building occupancy data of high resolution based on WiFi and BLE network, Autom. Constr. 102 (2019) 183–194, https://doi.org/10.1016/j.autcon.2019.02.016.
[29] B. Chaix, Mobile sensing in environmental health and neighborhood research, Annu. Rev. Public Health 39 (2018) 367–384, https://doi.org/10.1146/annurev-publhealth-040617-013731.
[30] E. Nemati, C. Batteate, M. Jerrett, Opportunistic environmental sensing with smartphones: a critical review of current literature and applications, Curr. Environ. Health Rep. 4 (2017) 306–318, https://doi.org/10.1007/s40572-017-0158-8.
[31] S. Aram, A. Troiano, E. Pasero, Environment sensing using smartphone, in: 2012 IEEE Sensors Applications Symposium Proceedings, 2012, pp. 1–4, https://doi.org/10.1109/SAS.2012.6166275.
[32] A. Bujari, O. Gaggi, C.E. Palazzi, A mobile sensing and visualization platform for environmental data, Pervas. Mobile Comput. 66 (2020), 101204, https://doi.org/10.1016/j.pmcj.2020.101204.
[33] J.S. Apte, K.P. Messier, S. Gani, M. Brauer, T.W. Kirchstetter, M.M. Lunden, J. D. Marshall, C.J. Portier, R.C.H. Vermeulen, S.P. Hamburg, High-resolution air pollution mapping with google street view cars: exploiting big data, Environ. Sci. Technol. 51 (2017) 6999–7008, https://doi.org/10.1021/acs.est.7b00891.
[34] A. Anjomshoaa, P. Santi, F. Duarte, C. Ratti, Quantifying the spatio-temporal potential of drive-by sensing in smart cities, J. Urban Technol. 28 (2021) 199–216, https://doi.org/10.1080/10630732.2020.1791679.
[35] Y. Leung, Y. Zhou, K.-Y. Lam, T. Fung, K.-Y. Cheung, T. Kim, H. Jung, Integration of air pollution data collected by mobile sensors and ground-based stations to derive a spatiotemporal air pollution profile of a city, Int. J. Geogr. Inf. Sci. 33 (2019) 2218–2240, https://doi.org/10.1080/13658816.2019.1633468.
[36] H. Guo, G. Dai, J. Fan, Y. Wu, F. Shen, Y. Hu, A mobile sensing system for urban PM2.5 monitoring with adaptive resolution, J. Sensors 2016 (2016) 7901245, https://doi.org/10.1155/2016/7901245.
[37] X. Zhou, A. Montazeri, J.D. Albertson, Mobile sensing of point-source gas emissions using Bayesian inference: an empirical examination of the likelihood function, Atmos. Environ. 218 (2019), 116981, https://doi.org/10.1016/j.atmosenv.2019.116981.
[38] X.-x. Chen, J. Huang, Odor source localization algorithms on mobile robots: a review and future outlook, Robot. Auton. Syst. 112 (2019) 123–136, https://doi.org/10.1016/j.robot.2018.11.014.
[39] K. Guo, P. Yang, D.H. Guo, Y. Liu, Gas leakage monitoring with mobile wireless sensor networks, Proc. Comput. Sci. 154 (2019) 430–438, https://doi.org/10.1016/j.procs.2019.06.061.
[40] D. Heinzerling, S. Schiavon, T. Webster, E. Arens, Indoor environmental quality assessment models: a literature review and a proposed weighting and classification scheme, Build. Environ. 70 (2013) 210–222, https://doi.org/10.1016/j.buildenv.2013.08.027.
[41] J.-H. Choi, V. Loftness, A. Aziz, Post-occupancy evaluation of 20 office buildings as basis for future IEQ standards and guidelines, Energy Build. 46 (2012) 167–175, https://doi.org/10.1016/j.enbuild.2011.08.009.
[42] C. Candido, J. Kim, R. de Dear, L. Thomas, BOSSA: a multidimensional post-occupancy evaluation tool, Build. Res. Inform. 44 (2016) 214–228, https://doi.org/10.1080/09613218.2015.1072298.
[43] C.M. Chiang, P.C. Chou, C.M. Lai, Y.Y. Li, A methodology to assess the indoor environment in care centers for senior citizens, Build. Environ. 36 (2001) 561–568, https://doi.org/10.1016/S0360-1323(00)00024-X.
[44] B.R.K. Mantha, M.K. Jung, B. García de Soto, C.C. Menassa, V.R. Kamat, Generalized task allocation and route planning for robots with multiple depots in indoor building environments, Autom. Constr. 119 (2020), 103359, https://doi.org/10.1016/j.autcon.2020.103359.
[45] M. Jin, S. Liu, S. Schiavon, C. Spanos, Automated mobile sensing: towards high-granularity agile indoor environmental quality monitoring, Build. Environ. 127 (2018) 268–276, https://doi.org/10.1016/j.buildenv.2017.11.003.
[46] Y. Yang, J. Liu, W. Wang, Y. Cao, H. Li, Incorporating SLAM and mobile sensing for indoor CO2 monitoring and source position estimation, J. Clean. Prod. 291 (2021), 125780, https://doi.org/10.1016/j.jclepro.2020.125780.
[47] K. Qian, X. Ma, X. Dai, F. Fang, B. Zhou, Gaussian process based IAQ distribution mapping using an interactive service robot, J. Ambient Intel. Smart Environ. 8 (2016) 359–373, https://doi.org/10.3233/AIS-160376.
[48] W.-Y. Wu, Y.-C. Liu, Autonomous guided robotic systems in regulating indoor environmental quality, in: 2018 IEEE/ASME International Conference on Advanced Intelligent Mechatronics (AIM), 2018, pp. 188–193, https://doi.org/10.1109/AIM.2018.8452331.
[49] Z. Hu, T. Song, K. Bian, L. Song, Deep reinforcement learning based indoor air quality sensing by cooperative mobile robots, in: 2020 IEEE Wireless Communications and Networking Conference (WCNC), 2020, pp. 1–6, https://doi.org/10.1109/WCNC45663.2020.9120611.
[50] Z. Hu, S. Cong, T. Song, K. Bian, L. Song, AirScope: mobile robots-assisted cooperative indoor air quality sensing by distributed deep reinforcement learning, IEEE Internet Things J. 7 (2020) 9189–9200, https://doi.org/10.1109/JIOT.2020.3004339.
[51] P. Kim, J. Chen, Y.K. Cho, SLAM-driven robotic mapping and registration of 3D point clouds, Autom. Constr. 89 (2018) 38–48, https://doi.org/10.1016/j.autcon.2018.01.009.
[52] J. Li, A.D. Heap, Spatial interpolation methods applied in the environmental sciences: a review, Environ. Model Softw. 53 (2014) 173–189, https://doi.org/10.1016/j.envsoft.2013.12.008.
[53] Q. Feng, C. Zhang, J. Lu, H. Cai, Z. Chen, Y. Yang, F. Li, X. Li, Source localization in dynamic indoor environments with natural ventilation: an experimental study of a particle swarm optimization-based multi-robot olfaction method, Build. Environ. 161 (2019), 106228, https://doi.org/10.1016/j.buildenv.2019.106228.